Role of Crystalline Defects in Electrocatalysis: CO Adsorption and Oxidation on Stepped Platinum Electrodes As Studied by in situ Infrared Spectroscopy

N. P. Lebedeva,*,† A. Rodes,‡ J. M. Feliu,‡ M. T. M. Koper,† and R. A. van Santen†

Schuit Institute of Catalysis, Laboratory of Inorganic Chemistry and Catalysis, Eindhoven University of Technology, 5600 MB Eindhoven, The Netherlands, and Departamento de Quimica Fisica, Universidad de Alicante, Apartado 99, E-03080 Alicante, Spain

Received: February 7, 2002; In Final Form: June 5, 2002

The adsorption of CO and the electrochemical oxidation of a CO adlayer on stepped Pt electrodes, Pt(443), Pt(332), and Pt(322), has been studied using in situ infrared reflection−absorption spectroscopy (IRAS). Coverage-dependent and potential-dependent spectra of CO adlayers on stepped Pt surfaces are reported. Infrared spectra acquired during oxidation of the CO adlayer provide information on the mechanism of the reaction and the structure of the operational catalytic active site. CO adsorbed on the (111) terraces is found to be more reactive compared to that adsorbed on either (110) or (100) steps. The step trough of either (110) or (100) step is concluded to be the active site for the electrocatalytic oxidation of the CO adlayer, the most reactive combination involving CO from the terrace and an oxygen-containing species in the step trough.

1. Introduction

In heterogeneous catalysis crystalline defects such as steps and kinks are known to be often more reactive than atoms in a flat surface.[1−3] The adsorption energy of many molecular and atomic adsorbates is higher on step- and kink sites, resulting in the preferential adsorption of species to surface atoms with a low coordination number (for example, carbon monoxide,[2−4] molecular and atomic oxygen,[5] nitric oxide, and atomic and molecular nitrogen[6]). Activation barriers for molecular dissociation reactions are often lower at step- and kink sites[5,6] compared to terraces, and these low-barrier reaction paths were found to totally dominate the reactivity in some cases.[6b,d] However, the catalytic effect of the step- and kink sites is not always caused by a lowering of the activation barrier of the reaction. In a recent study steps were found to be the active sites in oxygen dissociation on Pt without providing the lowest activation barrier.[7] The enhanced reactivity in this case could be related to a preferential adsorption of the oxygen molecule on the steps.

In electrocatalysis, steps and kinks are also known to be more reactive than flat surfaces. For example, a preferential adsorption of CO on both (100) and (110) steps on platinum has been observed at low CO coverages,[8−11] and also the oxidation of water to form surface oxygen-containing species in sulfuric acid solution on platinum is facilitated by all kinds of crystalline defects.[12] Steps of (110) orientation and crystalline defects were shown to catalyze CO oxidation on Pt[11,13−16] and Rh.[17] It has also been found that the dehydrogenation of formic acid is favored at both (100) and (110) steps, but since the CO formed adsorbs strongly at the steps the steady-state reactivity is low.[18] The same holds for the electrochemical oxidation of ethylene glycol[19] and ethanol.[20]

Since in many cases the reactivity of a heterogeneous catalyst depends sensitively on its structure, it is especially important to perform mechanistic studies on well-defined single-crystal surfaces. These model surfaces can be designed to expose varying densities and structures of atomic steps and/or kinks, thus allowing the systematic investigation of the influence of surface defects on the reaction kinetics and mechanism.[1]

CO oxidation on Pt single crystals is a model reaction that has been extensively studied for its fundamental as well as practical importance.[1−4] Both under ultrahigh vacuum (UHV) and electrochemical aqueous conditions the reaction has been found to be of the Langmuir−Hinshelwood type and involve two surface species—chemisorbed CO and an oxygen-containing species.[1−4,21−25] Steps were found to be active sites for the catalytic oxidation of a CO adlayer on stepped platinum surfaces.[2,26] To acquire more molecular level knowledge on the reaction mechanism one has to employ in situ spectroscopic techniques, such as infrared reflection−absorption spectroscopy (IRAS). The technique provides information on the chemical nature, concentration, and structure of the adsorbate both in UHV and under aqueous electrochemical conditions.[27−29] One of the advantages of IRAS is its ability to sensitively discriminate between adsorbates on different adsorption sites, i.e., steps and terraces. This makes infrared spectroscopy a powerful technique for catalyst surface characterization and in situ investigation of the nature and structure of the active sites.[26,30] Using in situ infrared spectroscopy Yates and co-workers demonstrated that for CO adlayer oxidation on Pt(533) in UHV, CO adsorbed on the terraces is more reactive compared to that on the steps, the most reactive combination involving a CO molecule from the terrace and an oxygen atom adsorbed in the step.[2,26]

Recently we have demonstrated quantitatively that the electrochemical oxidation of a CO adlayer on Pt also takes place uniquely on steps.[24,25] The goal of this study is to gain further insight into the reaction mechanism and the structure of the active site using in situ infrared spectroscopy. First, we present potential-dependent and coverage-dependent spectra of CO adlayers on several Pt stepped surfaces from both [1 $\bar{1}$ 0] and [0 $\bar{1}$ 1] zones. Next we report infrared spectra of the CO adlayer

* Corresponding author. Tel.: +31-40-247-4916. Fax: +31-40-245-5054. E-mail: N.P.Lebedeva@tue.nl.
† Eindhoven University of Technology.
‡ Universidad de Alicante.

10.1021/jp0203806 CCC: $22.00
Published on Web 08/30/2002

acquired during slow oxidation in a potential sweep, and we interpret these results using the band assignment from the first part of the paper.

2. Experimental Section

The platinum bead-type single crystals, diameter ca. 4 mm, were prepared according to the Clavilier method.[31] Two crystals of Pt[n(111) × (111)] (or equivalently Pt[(n − 1)(111) × (110)]) orientation, Pt(443) with n = 8 and Pt(332) with n = 6, and one of Pt[n(111) × (100)] orientation, Pt(322) with n = 5, were used in this study. Before each experiment the electrodes were flame annealed and cooled to room temperature in a H_2 + Ar atmosphere. After flame annealing, the single-crystal electrodes were transferred to the cell under the protection of a droplet of deoxygenated water. No protection of the crystal sides was used. A platinum wire was used as a counter electrode and a reversible hydrogen electrode was used as a reference.

A 0.1 M H_2SO_4 working solution was prepared from concentrated H_2SO_4 (Merck, "Suprapur") and ultrapure MilliQ water. Argon (N50) was used to deoxygenate all solutions and CO (N47) to dose CO.

The electrochemical infrared measurements were performed under external reflection conditions utilizing a Nicolet Magna 850 FTIR spectrometer equipped with a narrow-band liquid nitrogen-cooled mercury cadmium telluride (MCT) detector. The spectroelectrochemical cell[32] featured a prismatic CaF_2 window beveled at 60°. The cell and other glassware were cleaned by soaking in $KMnO_4$ solution overnight followed by rinsing with acidic H_2O_2 solution and repeated boiling in ultrapure water.[23]

Prior to each measurement the cyclic voltammogram of the working electrode in the supporting electrolyte was recorded to ensure the cleanliness of the system and crystalline order of the electrode surface. Adsorption of CO was performed from a dilute 10^{-5}−10^{-6} M CO solution, prepared by dosing an aliquot of 0.1 M H_2SO_4 saturated with CO into the cell. During the CO adsorption the working electrode was kept at 0.1 V in the bulk of the solution. After the exposure of the working electrode to CO-containing solution for a desired time, Ar was bubbled through the solution to remove dissolved CO. Then the electrode was returned into the meniscus mode and a cyclic voltammogram in the hydrogen adsorption region was recorded to estimate the number of the remaining surface sites available for hydrogen adsorption. A corresponding CO coverage, θ_{CO} (i.e., CO molecules per Pt surface atom), was then determined using the linear dependence of the hydrogen coverage on the CO coverage in the mixed hydrogen−CO adlayer,[24] which was established in a separate experiment for each working electrode. The CO coverages were calculated taking into account corrections for (bi)sulfate adsorption on the Pt(*hkl*) electrode in accordance with data obtained by the charge displacement technique.[33,34] After that, the electrode was positioned against the optical window.

To acquire IRAS data of a stable layer of adsorbed CO on Pt(332), typically 100 interferograms at 8 cm^{-1} resolution were collected at 0.1, 0.2, 0.3, and 0.4 V, followed by a reference spectrum obtained at 0.8 V, where the oxidative removal of the CO adlayer is complete. A total of 200 interferograms were co-added for a CO adlayer on Pt(443) and Pt(322) under otherwise equal conditions.

In the study of the mechanism of CO electrooxidation, CO adlayers on Pt(332) and Pt(322) were slowly oxidized in a potential sweep at 0.5 mV/s and 1 mV/s, respectively, while the IR spectra were collected using a rapid scan function, which allowed us to collect 327 interferograms each 18.4 s at 8 cm^{-1} resolution for the oxidation of the CO adlayer on Pt(332) and 162 interferograms each 9.2 s for the oxidation of CO adlayer on Pt(322). The reference spectra were obtained at 0.8 V.

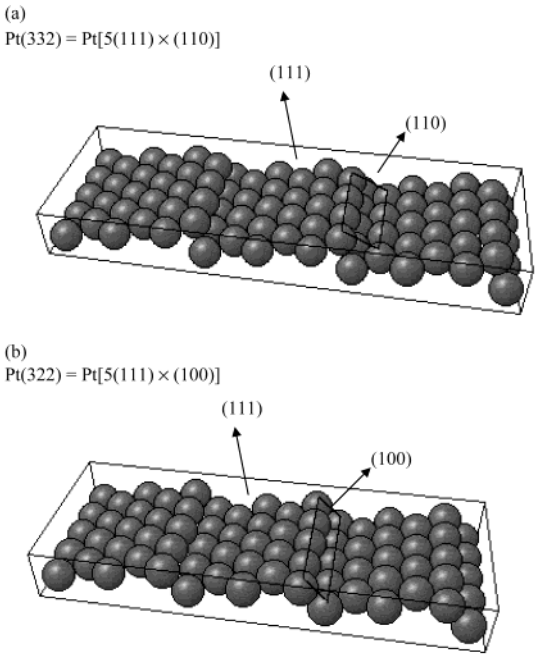

Figure 1. Schematic representation of Pt(332) (a) and Pt(322) (b) to illustrate the structure of the Pt[(n − 1)(111) × (110)] and Pt[n(111) × (100)] surfaces.[35]

3. Results and Discussion

3.1. Structure of the Electrode Surfaces and Their Voltammetric Profiles in CO-Free Electrolyte. The [(n − 1)(111) × (110)] surfaces for an fcc metal are composed of terraces of (111) orientation, which are (n − 1) atoms wide, separated by monatomic steps of (110) orientation (see Figure 1a[35]). The step geometry changes to (100) for the surfaces of [n(111) × (100)] orientation (Figure 1b[35]). These vicinal planes were found to be stable and have their nominal surface structure both under the UHV conditions[4a,c] and in air.[36] The specific electronic distribution at the stepped surfaces is known to result in significantly lower work functions of the stepped surfaces in UHV.[37] Recently, it was shown that the variation in work function of Pt stepped surfaces with step density was found not to be attenuated greatly by the presence of the aqueous ambient.[34] The quantitative agreement between the changes in the potential of zero change with the changes in work function observed in a vacuum as a function of step density, also attests to the equivalence of the surface structures of Pt[(n − 1)(111) × (110)] and Pt[n(111) × (100)] in the two environments. In the following, Pt(443), Pt(332), and Pt(322) are assumed to have their nominal step fractions, i.e., fraction of atoms on the step edge, $\theta_{step} = 1/n$, of 0.125, 0.167, and 0.2, respectively.

The pronounced structure sensitivity of the water reduction and oxidation to form adsorbed hydrogen- and oxygen-containing species and of anion adsorption and desorption processes enables the use of blank voltammetric profiles as a simple and sensitive tool to check and control the crystalline surface order of Pt(*hkl*) electrodes and the cleanliness of the system. It is now well established that the voltammetric profiles of Pt[(n − 1)(111) × (110)] in supporting electrolyte feature a characteristic peak at 0.125 V, which corresponds to the hydrogen adsorption and desorption on (110) steps.[38,39] A fingerprint of Pt[n(111) × (100)] surfaces is a peak at 0.28 V associated with the hydrogen adsorption and desorption on (100) step sites.[40]

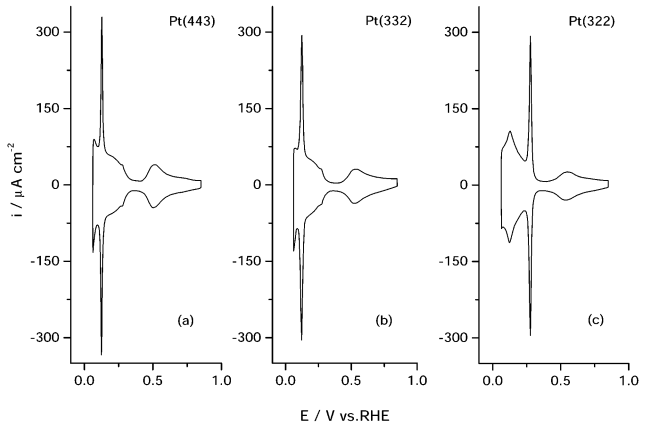

Figure 2. Cyclic voltammograms of the different Pt surfaces in 0.1 M H_2SO_4, sweep rate 100 mV/s, $T = 25$ °C. (a) Pt(443), (b) Pt(332), and (c) Pt(322).

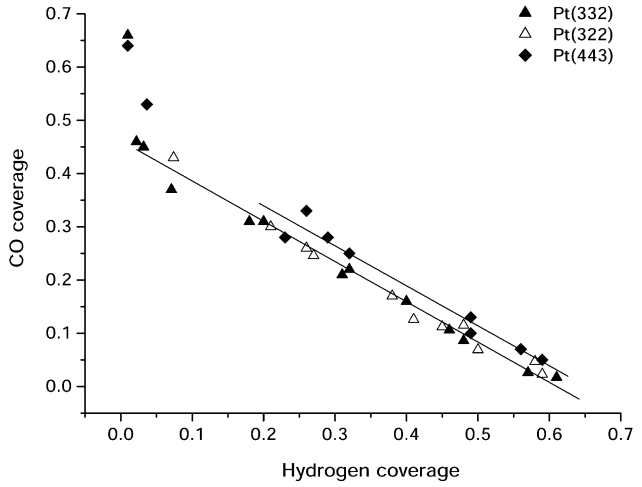

Figure 3. Relationship between the coverages of hydrogen and CO in the adlayer of the two coadsorbed species as measured from cyclic voltammetry for Pt(332) (filled triangles), Pt(322) (open triangles), and Pt(443) (diamonds), 0.1 M H_2SO_4, $T = 25$ °C. Solid lines are least-squares fits of the data.

Cyclic voltammograms of the stepped surfaces Pt(443), Pt(332), and Pt(322) are shown in Figure 2. The profiles are in good agreement with previously published data[34,38−40] confirming the surface crystalline order of the electrodes and the cleanliness of the system.

3.2. Coadsorption of CO and Hydrogen for CO Coverage Estimation. The initial CO coverage of an adlayer in the infrared measurements is often estimated from the integrated absorbance of the CO_2 band appearing at 2343 cm^{-1} as a result of adlayer oxidation.[45,46] This method has been successfully employed in the studies on large commercial crystals, since produced CO_2 remains essentially trapped in the thin-layer solution on the time scale of a typical IRAS experiment.[45,46] For longer experiments, such as the oxidation of an adlayer in a slow potential sweep, on small-area bead-type electrodes this approach might lead to the underestimation of the initial CO coverage due to nonnegligible diffusion of the CO_2 out of the thin layer. Therefore, we employed an alternative method for CO coverage estimation using the linear dependence of the hydrogen coverage on the CO coverage in the mixed hydrogen−CO adlayer.[24] Figure 3 shows the experimental relation between the hydrogen coverage and the CO coverage in the coadsorbed adlayer for Pt(332), Pt(443), and Pt(322). CO and hydrogen coverages were calculated from the corresponding voltammetric measurements of CO adlayer oxidation for the series of CO coverages (see Figure 4), taking into account corrections for (bi)sulfate adsorption on the Pt(*hkl*) electrode in accordance with data obtained by the charge displacement technique.[33,34] The hydrogen coverage decreases with increasing CO coverage, demonstrating that there is a competition between water and CO molecules for surface sites.[24,41,42] At CO coverages below ca. 0.5 the relationship is linear with a slope of ca. 0.8 for all surfaces. At higher CO coverage, water reduction to form adsorbed UPD hydrogen is completely blocked, but the CO uptake can still be increased and a number of CO coverages can be formed in the range between ca. 0.5 and saturation in agreement with previously reported data.[24,42] This clearly marks the range of CO coverages below 0.5 as the applicability region for our method of CO coverage estimation.

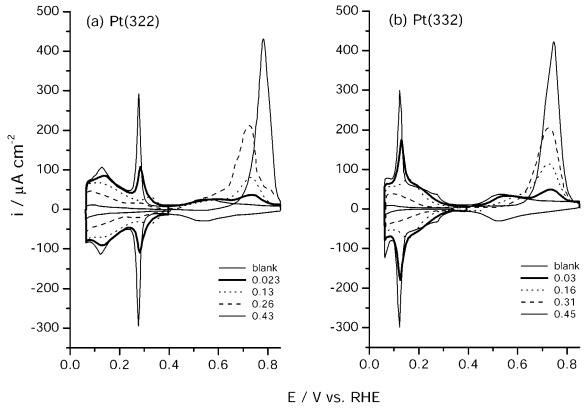

Figure 4. Voltammetric profiles of (a) Pt(322) and (b) Pt(332) in the presence of sub-saturated CO adlayers. 0.1 M H_2SO_4, sweep rate 100 mV/s, $T = 25$ °C, CO coverage is indicated in the figure.

Since the adsorption of CO and hydrogen on Pt is competitive, important information about the distribution of CO on the surface can be derived from the voltammetric profiles of the Pt(*hkl*) electrodes with a sub-saturated CO coverage (Figure 4). It can be seen that at low coverage CO blocks hydrogen adsorption on both (100) and (110) steps, while influencing hydrogen adsorption on (111) terraces only slightly. Therefore, we conclude that at low coverages CO adsorption preferentially takes place on steps, regardless of their structure. Our experimental results are consistent with UHV studies,[2,4,26] quantum chemical calculations,[3] and earlier studies of CO adsorption on Pt stepped surfaces in electrochemical environment,[8−11] where preferential CO adsorption on steps has been observed.

3.3. CO Adsorption. The IR spectra of CO adsorbed on Pt(443), Pt(332), and Pt(322) are shown in Figure 5, demonstrating the coverage dependence of the spectra at 0.1 and 0.4 V. In agreement with previously published data.[8−10,43,44] we observe two main vibrational bands for both Pt[$(n - 1)$(111) × (110)] and Pt[n(111) × (100)] orientations, which correspond to the stretching of atop and multifold coordinated CO. For both Pt(443) and Pt(332) these vibrational bands are observed at 2009−2075 cm^{-1} and 1786−1828 cm^{-1} for all CO coverages. For Pt(322) the band for atop CO is observed in the 1995−2075 cm^{-1} region and for multifold coordinated CO at 1795−1885 cm^{-1}, depending on the CO coverage and potential. All spectroscopic features blue-shift as usual with increasing CO coverage (see Figure 6) and potential (Figure 7).

3.3.1. Low CO Coverages. We begin the discussion of the spectra and assignment of the bands considering the spectra at low CO coverages, where CO is known to be predominantly adsorbed on steps, regardless of their orientation.[4,8−11]

A band around 2009−2030 cm^{-1} appears in the spectra for both Pt(443) and Pt(332) at CO coverages of 0.09 and 0.11−

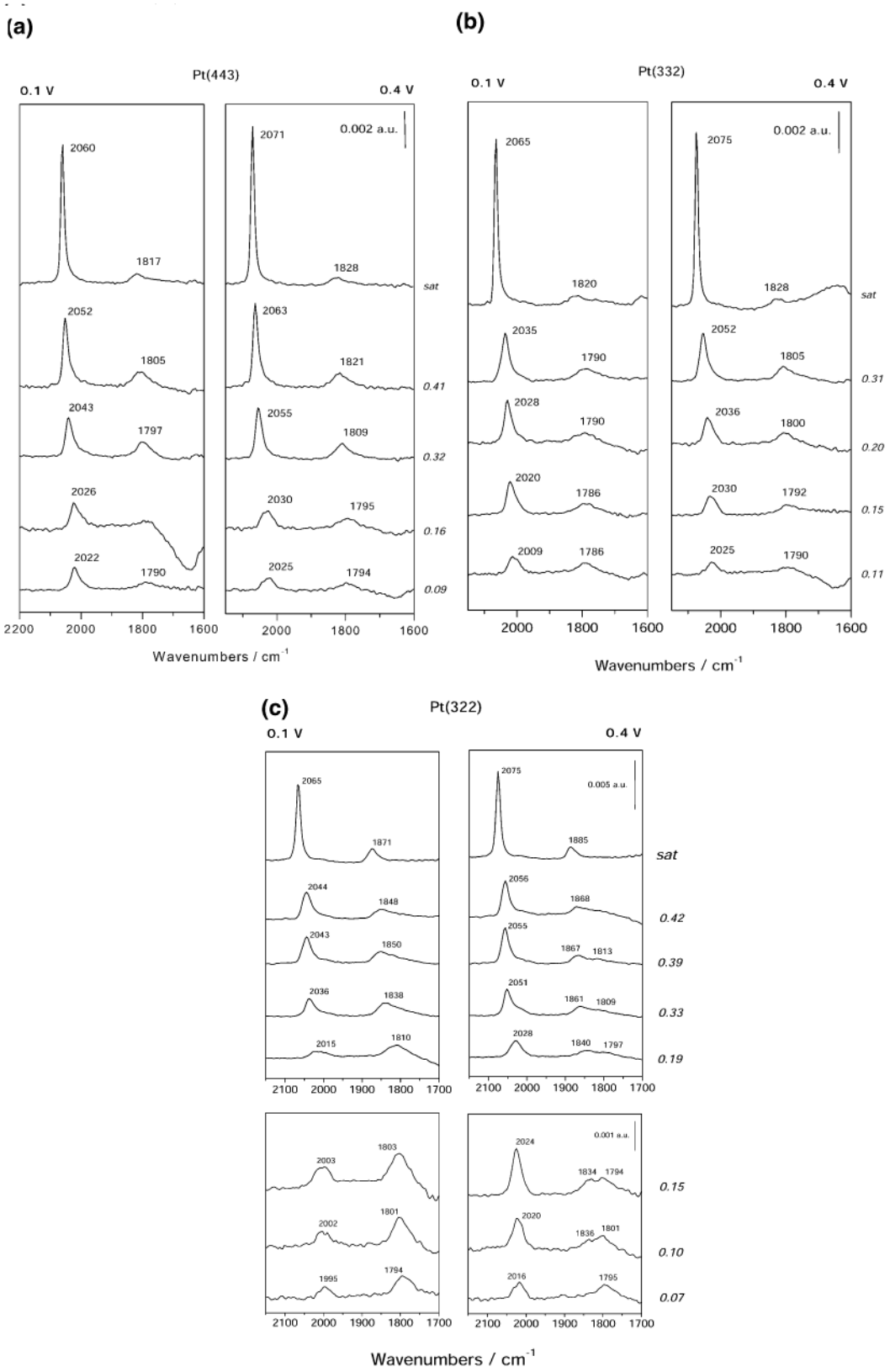

Figure 5. Infrared absorbance spectra of CO adsorbed on (a) Pt(443), (b) Pt(332), and (c) Pt(322) in 0.1 M H_2SO_4 at 0.1 and 0.4 V at the indicated CO coverages.

0.15, respectively (see Figure 5a,b). By comparing our data to the infrared spectra of CO adsorbed on Pt(997) in UHV[4c] we conclude that this band corresponds to the stretching of an atop-bound CO molecule on (110) steps. It is significantly red-shifted (ca. 20 cm^{-1}) with respect to the band of atop CO on Pt(111)[45,46] presumably due to enhanced back-donation at the low-coordinated step sites.[30] A second band is observed at 1786−1794 cm^{-1}, i.e., in the frequency region typical for 3-fold-hollow CO on Pt(111).[43,47] This mixture of CO molecules adsorbed in atop, and 3-fold-hollow configurations appear to be stable in

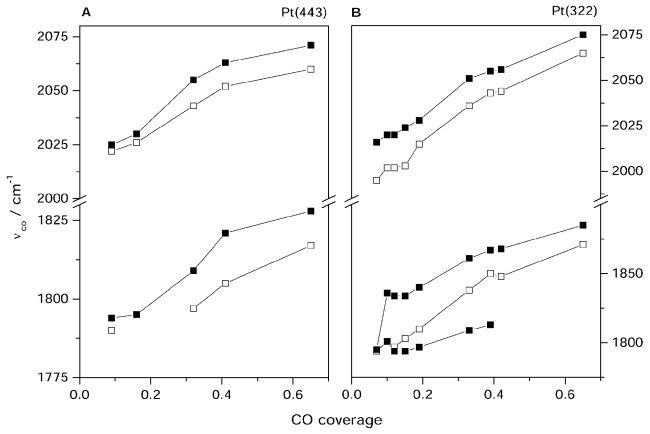

Figure 6. Peak frequencies of the CO band versus CO coverage for (A) Pt(443) and (B) Pt(322) at 0.1 V (open squares) and 0.4 V (filled squares).

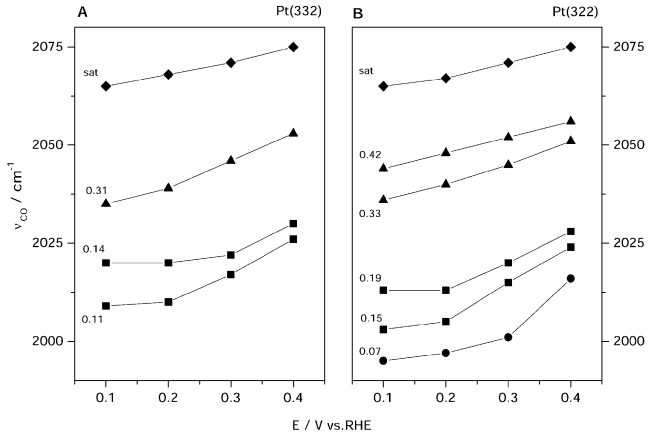

Figure 7. Peak frequencies of the CO band versus potential for (A) Pt(332) and (B) Pt(322) at indicated CO coverages.

the potential range 0.1−0.4 V and were observed systematically for both electrodes from the [1 $\bar{1}$ 0] zone at CO coverages below the saturation coverage of the step.

For low CO coverages on Pt(322) ($0.07 \leq \theta_{CO} \leq 0.15$) a band at 1995−2025 cm^{-1} is observed (Figure 5c), that was assigned to the vibration of atop CO adsorbed on (100) steps.[8−10,44] Similarly to CO on (110) steps, it is significantly red-shifted with respect to the band of atop CO on Pt(111). Interestingly, the spectral bands for atop CO adsorbed on (100) steps are also ca. 10 cm^{-1} red-shifted with respect to those for CO on (110) steps at all CO fractional coverages (see Figure 7). This might be a consequence of increased back-donation from the metal (100) steps to CO compared to (110) steps, although the role of varying steric repulsion cannot be ruled out.[50]

While a single feature at 1794−1803 cm^{-1} is observed at 0.1 V for low coverages of CO ($0.07 < \theta_{CO} < 0.15$), it splits into two poorly resolved bands at 1794−1801 cm^{-1} and ca. 1836 cm^{-1} at 0.4 V (Figure 5c). Taking into account the rather high local CO coverage on the steps in our experiments, the frequency of 1794−1803 cm^{-1} seems too low for this band to be assigned to bridge-bound CO (a band for bridge-bound CO on Pt(100) is observed at 1820−1870 cm^{-1} at ca. 0.1 V in the same range of CO coverages[48]). However, the band at ca. 1836 cm^{-1}, which appears at more positive potentials, is observed in the spectral region characteristic for the bridge-bound CO on Pt(100).[48] Therefore, we suggest that the band at 1794−1803 cm^{-1} corresponds to CO in the 3-fold-hollow configuration on the (100) step edge. Then, with increasing potential or CO coverage a restructuring of the adsorbate layer occurs with a partial transition of 3-fold-hollow CO to a bridge-bound CO, yielding an extra band at ca. 1836 cm^{-1}. It is surprising, however, that the two bands appear resolved, although the spectral separation is only ca. 30 cm^{-1}. A possible explanation is that the species are well separated in space, for instance, by an atop CO molecule.

In a series of publications Korzeniewski and co-workers reported a detailed study of the CO adsorption on Pt(533) and Pt(755) electrodes,[8−10,44] whose surface structures are homologous to that of Pt(322) studied in the present work. Our vibrational spectra are generally in good agreement with those presented in refs 8−10, indicating that the structure of the CO adlayer is similar for all these surfaces. However, there are some differences in band(s) position and assignment for the multi-fold CO. Similarly to the present study, adsorption of CO at low coverage on Pt(755) at potentials in the hydrogen region resulted in a single feature at 1799 cm^{-1}, which was observed to split into two bands at ca. 1800 and 1835 cm^{-1} as the potential was changed to the double layer region.[10] However, a single broad band at 1788−1821 cm^{-1} was observed for low CO coverages on Pt(533) at all potentials.[8,9] In both cases the bands were assigned to bridge-bound CO adsorbed on (100) steps. As discussed above we believe that the lower energy band is due to the 3-fold hollow CO.

Figure 8 shows the potential dependence of the vibrational spectra for CO adsorbed on (110) and (100) steps. There is a clear transition of multi-fold-coordinated CO into atop-bound CO on (100) steps with increasing potential as evidenced by the decrease of the intensity of the band at 1797−1834 cm^{-1} and increase of the intensity of the 2000−2020 cm^{-1} band (Figure 8c). A similar CO adlayer rearrangement on (100) steps was observed by Kim et al.[8−10] for Pt(533) and Pt(755) and was concluded to reflect the general tendency of CO toward high-coordination adsorption sites with more negative electrode potentials.[29,49] The latter is known to be a consequence of the higher back-donation to high-coordination sites from the metal to the CO $2\pi^*$ orbital as the potential is lowered.[29,49,50] A very different trend is observed for CO adsorbed on (110) steps (Figure 8a,b). The intensity of the band of atop CO at 2009−2025 cm^{-1} *decreases* with increasing potential, while the intensity of the spectral feature of the multi-fold coordinated CO is essentially potential-invariant (Figure 9). This effect is systematically observed for both Pt(443) and Pt(332) for CO coverages below 0.16 and 0.2, respectively (see Figures 5a,b and 8a,b), i.e., in the coverage range where CO is expected to occupy predominantly the step sites. No oxidative removal of CO was observed at these potentials as proved by the absence of the CO_2 band at 2343 cm^{-1}. Note that for the fractional CO coverages close and/or slightly higher than 1, the vibrational band of step-bound CO is still dominating the spectra and this explains why the effect of the unexpected variation of the band intensity with potential is observed even if CO begins to populate terraces.

Since the CO coverage is constant in the experiment described in the previous paragraph, we believe that the observed variation of the band intensity with potential may reflect a change in the CO−metal bonding with potential (or equivalently with the electric field across the electrical double layer). As it was first proposed by Kunimatsu, this complex effect can be qualitatively related to the decreasing back-donation from the metal to the $2\pi^*$ bonding orbital of CO with potential, which, in turn, may lower the dynamic dipole moment of CO and hence the intensity of the IR band of CO stretching.[51] This conclusion was further

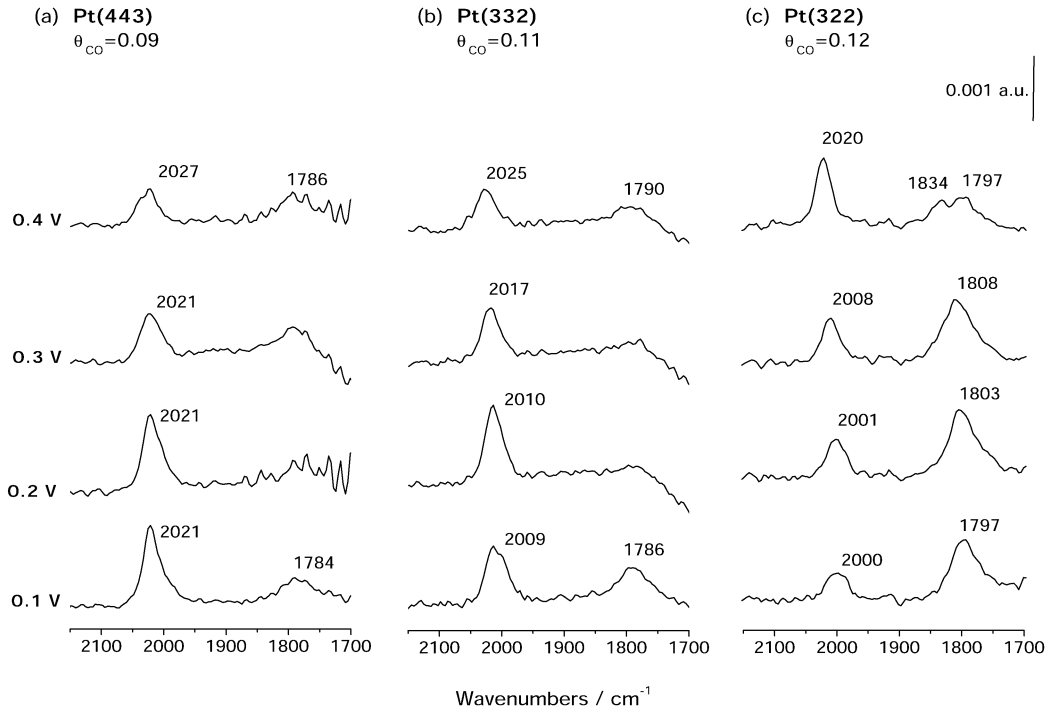

Figure 8. Potential dependence of the infrared absorbance spectra of CO at low adsorbate coverages. Surface orientation, CO coverages, and potential are indicated in the figure.

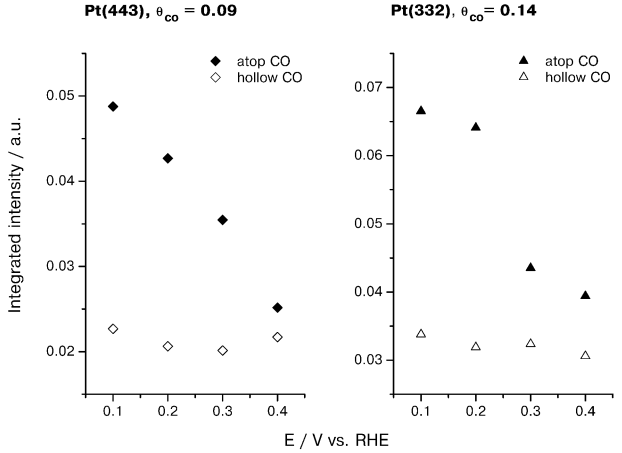

Figure 9. Potential dependence of the integrated band intensity for atop CO (filled symbols) and 3-fold hollow CO (open symbols) adsorbed on (110) steps. Surface orientation and CO coverages are indicated in the figure.

supported by ab initio calculations of the vibrational characteristics of CO adsorbed on Cu (100).[52] However, Bagus et al. attributed the change in the band intensity of CO on Pd(100) with applied field to the field-induced redistribution of the charge within the CO molecule itself.[53] It is now well established that both the so-called "chemical effect", i.e., the change of the extent of donation and back-donation with potential, and the "Stark effect", i.e., the field-induced redistribution of the electrons within the adsorbed molecule, cannot be considered separately.[50,52] For an adsorbate at the metal/electrolyte interface these processes are not independent and lead to what might be called the "interfacial Stark tuning effect". Recent DFT calculations showed that the dynamic dipole moment of different adsorbates depends sensitively on the field (potential), thus influencing the intensity of spectral bands.[54] These results, however, refer to the metal−adsorbate stretching and not to the CO internal stretching. There is only limited experimental evidence on the variation of the infrared band intensity with applied field (potential).[51,55−57] As has been pointed out by Lambert, other factors, such as site switching of the adsorbate with potential, CO tilting, and potential-dependent coadsorption of other species (hydrogen and/or anions), may interfere with the field-induced variation of the band intensity, making this phenomenon difficult to be observed unambiguously.[57] Since there is no conversion of multi-fold-bound CO into atop CO on (110) steps, we believe that this system is particularly suitable for an analysis of the intensity variation with potential. On the other hand, potential-dependent coadsorption of hydrogen takes place in our experiments and may influence the observations.

The potential dependence of the vibrational band position for atop CO adsorbed on either (110) or (100) steps is found to be nonlinear with a Stark tuning rate varying from almost zero at 0.1−0.2 V to ca. 80 cm^{-1}/V at 0.2−0.4 V (see Figure 7). Similar nonlinear and even nonmonotonic dependencies of the CO vibrational frequency on potential were reported previously for CO on Pt(533)[8] and supported Pt nanoparticles.[58]

3.3.2. Intermediate CO Coverages. As the CO coverage increases, CO begins to populate the terraces. A single band for atop CO on Pt(443), Pt(332), and Pt(322) is observed in the range of 2028−2063 cm^{-1} depending on the potential (Figure 5). Due to the dipole−dipole coupling of the vibrational modes of atop CO on steps and atop CO on the terraces, the bands for the two species are not well resolved. The presence of CO bound to the steps can be readily concluded from the asymmetry of the band exhibiting either a shoulder or a tailing on the low-frequency side (Figure 5). Since the vibrational frequency of CO adsorbed on (111) terraces is higher than that of the CO on steps, population of the terraces causes a significant blue shift of the spectral features of atop and multi-fold-coordinated CO. This is reflected by the characteristic S-type dependence of the CO vibrational frequency on the CO coverage (see Figure 6).[8]

Similar observations of significant vibrational coupling of the CO species on the terraces and on the steps were reported earlier by Kim et al. for CO adsorption on Pt(533).[8,9] However, contrary

to their observations, neither a splitting of the band into two bands, nor an increase of the intensity of the shoulder with potential was detected in our experiments. Interestingly, two separate bands were detected for a CO adlayer on Pt(755).[10] Hence, the population of the terraces of Pt(755) by CO was concluded to occur at random by Kim et al. in order to explain the lower coupling observed when compared to Pt(533).[10] The inability to discern the band of CO on the steps from that of CO on the terraces on Pt(533) was attributed to the interactions between the adsorbed CO layer and the aqueous electrochemical environment.[8]

Since the degree of dipole−dipole coupling between step and terrace CO is significant even for low CO coverage on the terrace in our experiments, it is tempting to propose that the occupation of the terraces takes place via a successive filling of the rows starting with the sites closest to the steps. A higher residence time of CO on the terrace close to the step caused by a slightly higher adsorption energy of CO there would be a possible explanation. However, this hypothesis does not seem to be consistent with the existing UHV data. Two well-resolved bands for CO on terraces and steps were observed in the corresponding UHV measurements of CO adsorbed on Pt(533) at 90 K.[2,4a,26] By contrast, CO on steps was found to be significantly vibrationally coupled to CO on the terraces on Pt(997) at 300 K,[4c] where the adsorbed CO is expected to be much more mobile and less localized in the hypothetically more favorable position in the step vicinity. Moreover, the CO−CO lateral interaction is known to be repulsive and CO has been shown to be highly mobile on the (111) terraces both under UHV[59] and aqueous electrochemical conditions.[23−25] This suggests that the observed vibrational coupling between CO on steps and terraces is unlikely to be related to a preferential occupation of the terrace site close to the steps and originates from a different phenomenon. Insufficient spatial separation of the species on the step and in the middle of the terrace also cannot fully account for the observed vibrational coupling, since it has been detected in UHV for Pt(997)[4c] and under aqueous electrochemical conditions for Pt(443) in the present study, both surfaces having rather large ca. 20 Å wide terraces.

At intermediate CO coverages the dependence of the CO vibrational frequency on potential becomes almost linear for both crystal orientations with a Stark tuning rate of about 50−60 cm^{-1}/V at $\theta_{CO} = 0.30-0.35$ and ca. 40 cm^{-1}/V at $\theta_{CO} = 0.40-0.45$ in agreement with previous observations.[8]

Bridge-bound CO also appears on the terraces with increasing CO coverage and, through the dipole−dipole coupling of the vibrational modes and intensity stealing, this results into two apparently different effects for the $[(n-1)(111) \times (110)]$ and $[n(111) \times (100)]$ orientations. On Pt(443) and Pt(332) the vibrational feature at 1790−1821 cm^{-1} blue shifts progressively with increasing CO coverage, finally reaching the position of 1820−1828 cm^{-1} characteristic for bridge-bound CO on Pt(111) terraces[46] (Figure 5a,b). The multi-fold CO on (110) steps is seen again as a low-frequency "tail" of the main band. By contrast, the vibrational feature at 1840−1868 cm^{-1}, related to the bridge-bound CO on (100) steps, is dominating the spectra for Pt(322).[8−10] Its intensity increases significantly at the expense of the band of bridge-bound CO on terraces, which is now lower in frequency.[8−10] Apparently, CO bound to a hollow site on (100) steps survives up to relatively high CO coverages and does not convert into bridge-coordinated species as evidenced by the presence of a low-frequency shoulder of the main band at 0.1 V and a separate band at 1797−1813 cm^{-1} at 0.4 V (Figure 5c).

3.3.3. Saturated CO Coverages. At saturated CO coverages (typically ca. 0.65 for stepped Pt surfaces studied here) a band at 2060−2075 cm^{-1} and a much weaker feature at 1817−1828 cm^{-1} are present in the spectra for both electrodes of $(n-1)(111) \times (110)$ orientation. Similar spectra were reported in a recent work of Rodes et al.[43] However, Hoshi et al. observed only one spectral band at 2069−2072 cm^{-1} for CO adsorbed on the Pt$[(n-1)(111) \times (110)]$ electrodes with $n \leq 8$ even in the presence of CO in the solution.[60] The band at 2060−2075 cm^{-1} can be clearly related to the combination of atop CO on (111) terraces and (110) steps, with the former component dominating the spectra.[30,43] The feature at 1817−1828 cm^{-1} was ascribed by Rodes et al.[43] to the stretching of bridge CO on the (111) terrace, since a systematic replacement of a 3-fold-hollow by a bridge feature was observed for surfaces with progressively narrower (111) terraces. Although we also adhere to this assignment here, there may be a contribution of the multi-fold coordinated CO on (110) steps, similarly to the case of the intermediate CO coverages.

For the surface with (100) steps a pair of IR bands appears at 2065−2075 and 1870−1885 cm^{-1} in agreement with the previous work of Korzeniewski and co-workers[8−10,44] and Rodes et al.[43] Similarly to the case of the Pt$[(n-1)(111) \times (110)]$ surfaces, the first band is commonly related to a combination of atop CO on (111) terraces and on (100) steps, with the latter component being indiscernible due to the dipole−dipole coupling of the vibrational modes.[8−10,30,43,44] The second feature observed at 1870−1885 cm^{-1} is indicative of the presence of bridge-bound CO on (100) steps and (111) terraces, with the former feature dominating the spectra due to the dipole−dipole coupling and intensity stealing (vide supra).

3.4. CO Oxidation. Figure 10 shows a series of vibrational spectra recorded during the oxidation of a sub-saturated CO adlayer on Pt(322) and Pt(332) in a slow potential sweep. Initially, in the spectral region for atop CO only one band at ca. 2050 cm^{-1} with a shoulder on the low-frequency side is observed for both electrodes. As discussed in the previous section, this feature is indicative of the coexistence of atop CO on the terraces and steps, with the former component dominating through the dipole−dipole coupling of the vibrational modes and intensity stealing from the latter one.

A splitting of this band into two clearly resolved features at 2050−2060 cm^{-1} and 2025−2030 cm^{-1}, corresponding to atop CO on the (111) terraces and (100) steps (vide supra), was reproducibly observed upon the incipient oxidation of CO adlayer on Pt(322) (Figure 10a). The intensity of the latter band is increased compared to that of the shoulder of the parent feature (Figure 10a). A very similar, albeit less pronounced, effect is observed for the oxidation of CO adlayer on Pt(332) (Figure 10b). No separate band of atop CO on (110) steps emerges, only a shoulder at ca. 2030 cm^{-1} on the low-frequency side of the main band becomes more pronounced upon oxidation of CO (Figure 10b).

These observations demonstrate that the vibrational coupling is lifted upon the incipient oxidation of CO and the two species remain essentially independent (at least in the case of (100) steps) until the entire adlayer is stripped off. This can only be possible if the species with higher frequency, i.e., CO adsorbed on the terraces, is spatially well separated from the lower frequency one, i.e., CO on steps. We have shown recently that the oxidation of a CO aldayer on Pt stepped electrodes takes place preferentially at the steps.[24,25] Taking into account the results illustrated in Figure 10, we conclude that CO adsorbed on the (111) terraces reacts first, leaving CO on either (100) or

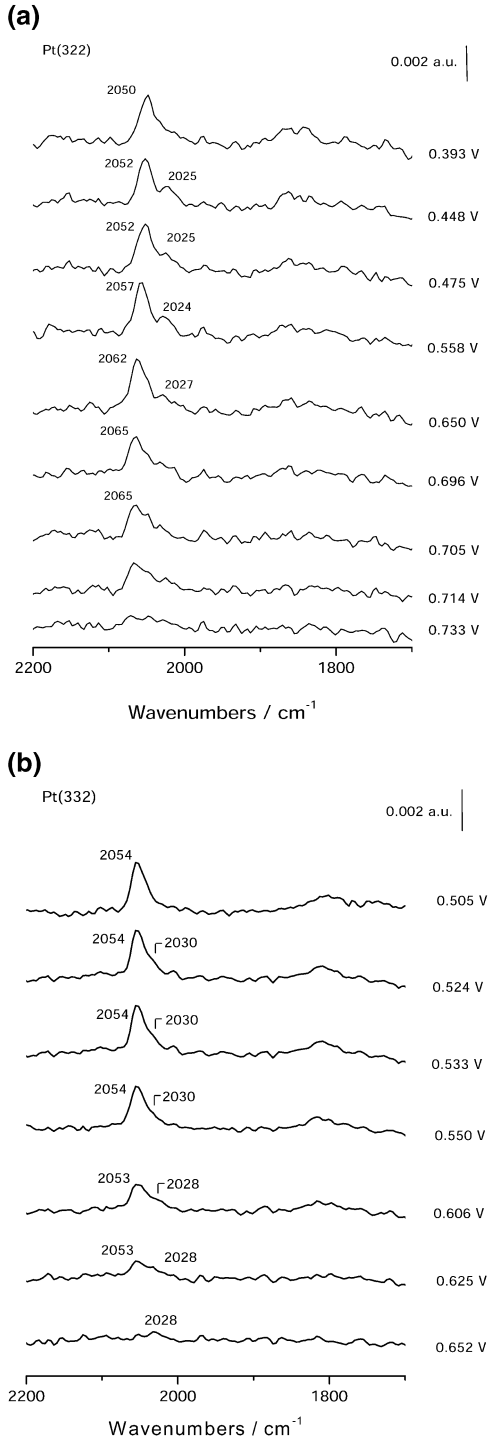

Figure 10. Series of infrared spectra acquired during CO adlayer oxidation in a potential sweep in 0.1 M H_2SO_4. (a) Pt(322), initial CO coverage 0.33; starting potential 0.2 V, sweep rate 1 mV/s, reference spectrum potential 0.8 V; (b) Pt(332), initial CO coverage 0.34; starting potential 0.45 V, sweep rate 0.5 mV/s, reference spectrum potential 0.8 V. The top spectrum in both series represents a fingerprint of the stable adlayer at the corresponding potential (no CO oxidation), all following spectra were acquired with oxidation in progress.

(110) steps behind. The low reactivity of CO on the steps is not surprising taking into account its significantly higher (ca. 35 kJ/mol) adsorption energy compared to CO on the terrace.[2,4] The alternative scenario of the CO adsorbed on steps reacting first does not seem to be consistent with the experimental results shown in Figure 10. In this case the step sites which are becoming vacant due to the oxidation of CO from the steps, would be rapidly re-occupied by CO from the terrace via fast diffusion. Therefore, the local arrangement of the CO species at the active site during the reaction would not differ from the initial configuration of the CO molecules in the stable adlayer, and, hence, no splitting of the IR band should be observed.

As the reaction proceeds the intensity of the band at ca. 2050−2060 cm^{-1}, assigned to the CO on the terraces, decreases faster than that of the band of CO on steps at 2025−2030 cm^{-1} (Figure 10). It is known that the intensity of the infrared band can hardly be considered quantitatively due to the complex interactions between different coadsorbed species.[29,30] Nevertheless, this observation supports the idea of a higher reactivity of CO adsorbed on terraces, since even intensity borrowing from the low-frequency component does not prevent the dominating band from diminishing faster than the low-frequency partner. The position of the high-frequency band shifts to slightly higher wavenumbers from 2050 to 2065 cm^{-1} during the CO oxidation on Pt(322), while it is time and potential invariant in the case of Pt(332). Usually, the presence of a hysteresis in the band position during CO dosing and oxidation is interpreted in terms of island formation.[29,46,48] It is difficult to conclude whether CO islands are formed in the present case, since two counteracting factors, namely, increasing potential, which blue shifts the band, and decreasing CO coverage, which red shifts the band, are interfering.

The remaining question is whether the step edge or the inner corner is active in electrocatalytic oxidation of adsorbed CO. The answer may be proposed from the comparison of the series of vibrational spectra of CO oxidation on Pt(322) and Pt(332). These two surface orientations differ mainly in the structure of the step trough and it would be logical to link the observed spectral differences to this structural dissimilarity. One of the parameters that vary with the step structure is the distance between the step edge and the nearest atom on the lower terrace. For the hard-spheres surface model it is 1.3 times longer for the (110) step compared to the (100) step (6.2 Å compared to 4.8 Å, respectively). CO adsorbed on the (100) step is likely to be vibrationally coupled with CO molecules on both upper and lower terraces (Figure 11). While CO on (110) steps is also coupled with its neighbors from the upper terrace, it should "feel" the presence the CO molecules on the lower terrace about 2 times less due to 1.3 times greater spatial separation between them compared to the (100) steps (Figure 11). (The extent of vibrational coupling decreases as $1/R^3$, where R is the distance between the species[28]). Hence, the oxidative removal of CO molecules adsorbed on the upper terrace would influence the spectra of CO adlayer on both Pt(332) and Pt(322) electrodes in a similar fashion. However, the oxidation of CO from the lower terrace should affect the vibrational characteristics of the CO on (110) steps less compared to those of CO on (100) steps. Our experimental data are supportive of the latter hypothesis: while a clear splitting of the band is detected during the CO oxidation on Pt(322), only a shoulder related to CO on (110) steps is observed to become more pronounced (see Figure 10). This suggests that it is the inner corner of the step that is active in the CO electrooxidation. It has been shown in our previous voltammetric study of the CO adlayer oxidation on stepped Pt surfaces that steps enhance the formation of the oxygen-containing species at low potentials.[11] We also proposed that the oxidative water decomposition occurs preferentially in the step trough.[11] The lifting of the vibrational coupling between CO on steps and terraces in the course of oxidation may then be due to the adsorption of oxygen-containing species in the

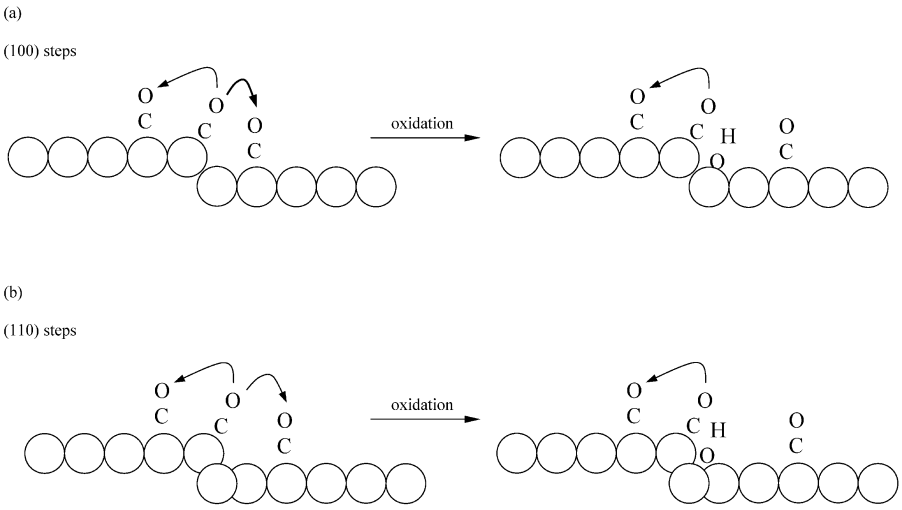

Figure 11. Schematic representation of the dipole−dipole coupling of CO on steps with CO on the terraces and its lifting upon the initial adlayer oxidation.

step's trough, preventing CO from adsorbing in the step vicinity (Figure 11).

The active site and the corresponding arrangement of reacting species proposed here for the electrochemical oxidation of the CO adlayer are quite similar to those for the oxidation of CO under the UHV conditions. In a UHV study of the mechanism of the CO adlayer oxidation on Pt(533) Yates et al. demonstrated that CO chemisorbed on the (111) terrace is more reactive than CO adsorbed on the (100) steps, while the reverse is true for oxygen chemisorbed in the 4-fold-hollow site in the (100) step.[2,26] The most reactive combination was therefore concluded to be oxygen adsorbed in the step and CO adsorbed on the nearest terrace site.[2,26] Two possible reasons for the high reactivity of this pair were proposed. First, the lower adsorption energy of CO on the terrace compared to that of CO on the steps supposedly leads to a lower activation barrier for its oxidation.[2,26] The second reason was a favorable geometric arrangement of the reacting particles that resulted in a short approach distance, which was proposed to lower the activation barrier as well.[2,26] Both arguments can presumably be applied to the reaction taking place under aqueous electrochemical conditions.

From the above we conclude that CO adsorbed on the terraces is more reactive than CO on steps and it reacts away first, leaving CO on either (100) or (110) steps behind. The reaction is expected to take place in the step trough, which is accessible for water oxidation to form the oxygen-containing species with which CO reacts. CO adsorbed on the steps oxidizes slowly and apparently mainly through the conversion into "terrace" CO and fast diffusion to the active site, but not through reaction with the oxygen-containing species directly at the step.[61] This mechanism is also similar to that suggested for CO oxidation on stepped Pt surfaces in UHV.[2,26] The slow oxidation of CO on steps may explain the "tailing" observed in the chronoamperometric transients of CO oxidation on Pt stepped surfaces with relatively narrow terraces and a high concentration of steps.[25,61]

4. Conclusions

The adsorption of CO and the electrochemical oxidation of a CO adlayer on stepped Pt electrodes—Pt(443) = Pt[7(111) × (110)], Pt(332) = Pt[5(111) × (110)], and Pt(322) = Pt[5(111) × (100)]—have been studied using in situ infrared reflection−absorption spectroscopy (IRAS).

At low coverages CO is found to adsorb preferentially on both (110) and (100) steps in agreement with previous experimental studies of CO adsorption on Pt stepped surfaces under UHV conditions and in electrochemical environment, as well as with quantum chemical calculations. The spectral features of CO adsorbed on the step sites are significantly (ca. 20 cm^{-1}) red-shifted with respect to the corresponding vibrational modes of CO on the terraces presumably due to the enhanced back-donation to CO on those sites. A mixture of CO in atop and 3-fold hollow configurations is observed throughout the 0.1−0.4 V potential region for both electrodes with (110) steps. The band intensity of atop-bound CO on (110) is found to decrease with increasing potential. This effect may be related to a change of the CO internal dynamic dipole moment with potential. For (100) steps the site occupancy of CO is potential and coverage dependent. At low fractional CO coverages ($\theta_{CO}/\theta_{step}$) the adlayer features both atop and 3-fold-hollow CO. The latter species converts into bridge-bound CO at increased potential and/or CO coverage.

Both atop and multi-coordinated CO species are detected in the CO adlayer at intermediate and saturated CO coverages for all Pt surfaces studied. Vibrational coupling between CO on steps and terraces, along with intensity borrowing, is observed to play a significant role at intermediate and saturated CO coverages, leading to the predominant detection of features related to the CO species on the terraces.

Infrared spectra acquired during oxidation of the CO adlayer provide information on the mechanism of the electrochemical oxidation of a CO adlayer on platinum and the structure of the catalytic active site operational in this reaction. We have shown that, similarly to catalytic oxidation of adsorbed CO on platinum in UHV, CO adsorbed on the (111) terraces is more reactive compared to CO on either (110) or (100) steps. Oxidative water decomposition forming the oxygen-containing species needed for CO oxidation is likely to occur in the step trough. The latter species apparently prevents CO from adsorbing on terrace sites near the step trough as inferred from the lifting of the vibrational coupling between CO on terraces and steps after the initial adlayer oxidation. Thus, the inner corner of either (110) or (100) step is concluded to be the active site for the electrocatalytic oxidation of the CO adlayer and the most reactive combination involves CO from a near-step terrace site and the oxygen-containing species in the step trough. CO from the steps reacts

slowly and apparently mainly through the conversion into "terrace" CO and subsequent fast diffusion to the active site.[61]

Acknowledgment. Helpful discussions with Professor H. Baltruschat are gratefully acknowledged. This research was supportedby the Royal Netherlands Academy of Arts and Sciences (KNAW), by a Spinoza grant from The Netherlands Foundation for Scientific Research (NWO), and by the Ministerio de Ciencia y Tecnologia (Spain) Grant BQU 2000-0240.

References and Notes

(1) Somorjai, G. A. *Introduction to Surface Chemistry and Catalysis*; John Wiley & Sons: New York, 1994.
(2) Yates, J. T., Jr. *J. Vac. Sci. Technol. A* **1995**, *13*, 1359.
(3) Hammer, B.; Nørskov, J. K. *Adv. Catal*. **2000**, *45*, 71.
(4) (a) Hayden, B. E.; Kretzschmar, K.; Bradshaw, A. M.; Greenler, R. G. *Surf. Sci*. **1985**, *149*, 394. (b) Luo, J. S.; Tobin, R. G.; Lambert, D. K.; Fisher, G. B.; DiMaggio, C. L. *Surf. Sci*. **1992**, *274*, 53. (c) Hahn, E.; Fricke, A.; Roder, H.; Kern, K. *Surf. Sci*. **1993**, *297*, 19. (d) Wang, H.; Tobin, R. G.; Lambert, D. K. *J. Chem. Phys.* **1994**, *101*, 4277. (e) Hammer, B.; Nielsen, O. H.; Nørskov, J. K. *Catal. Lett.* **1997**, *46*, 31.
(5) (a) Gland, J. L.; Korchak, V. N. *Surf. Sci.* **1978**, *75*, 733. (b) Feibelman, P. J.; Esch, S.; Michely, T. *Phys. Rev. Lett.* **1996**, *77*, 2257. (c) Wang, H.; Tobin, R. G.; Lambert, D. K.; DiMaggio, C. L.; Fisher G. B. *Surf. Sci*. **1997**, *372*, 267.
(6) (a) Ramsier, R. D.; Gao, Q.; Neergaard Waltenburg, H.; Yates, J. T., Jr. *J. Chem. Phys.* **1994**, *100*, 6837. (b) Zambelli, T.; Wintterlin, J.; Trost, J.; Ertl, G. *Science* **1996**, *273*, 1688. (c) Hammer, B. *Faraday Discuss*. **1998**, *110*, 323. (d) Dahl, S.; Logadottir, A.; Egeberg, R. C.; Larsen, J. H.; Chorkendorff, I.; Törnqvist, E.; Nørskov, J. K. *Phys. Rev. Lett*. **1999**, *83*, 1814. (e) Hammer, B. *Surf. Sci*. **2000**, *459*, 323.
(7) Gambardella, P.; Šljivančanin, Ž.; Hammer, B.; Blanc, M.; Kuhnke, K.; Kern, K. *Phys. Rev. Lett*. **2001**, *87*, 56103.
(8) Kim, C. S.; Tornquist, W. J.; Korzeniewski, C. *J. Phys. Chem.* **1993**, *97*, 6484.
(9) Kim, C. S.; Korzeniewski, C.; Tornquist, W. J. *J. Chem. Phys*. **1994**, *100*, 628.
(10) Kim, C. S.; Korzeniewski, C. *Anal. Chem.* **1997**, *69*, 2349.
(11) Lebedeva, N. P.; Koper, M. T. M.; Herrero, E.; Feliu, J. M.; van Santen, R. A. *J. Electroanal. Chem.* **2000**, *487*, 37.
(12) (a) Motoo, S.; Furuya, N. *J. Electroanal. Chem*. **1984**, *172*, 339. (b) Clavilier, J.; El Achi, K.; Petit, M.; Rodes, A.; Zamakhchari, M. A. *J. Electroanal. Chem.* **1990**, *295*, 333.
(13) Love, B.; Lipkowski, J. *ACS Symp. Ser*. **1988**, *378*, 484.
(14) Santos, E.; Leiva, E. P. M.; Vielstich, W. *Electrochim. Acta* **1991**, *36*, 555.
(15) Petukhov, A. V.; Akemann, W.; Friedrich, K. A.; Stimming, U. *Surf. Sci*. **1998**, *402*−*404*, 182.
(16) Lebedeva, N. P.; Koper, M. T. M.; Feliu, J. M.; van Santen, R. A. *Electrochem. Commun.* **2000**, *2*, 487.
(17) Gómez, R.; Orts, J. M.; Feliu, J. M.; Clavilier, J.; Klein, L. H. *J. Electroanal. Chem.* **1997**, *432*, 1.
(18) (a) Motoo, S.; Furuya, N. *Ber. Bunsen-Ges. Phys. Chem.* **1987**, *91*, 457. (b) Smith, S. P. E.; Ben-Dor, K. F.; Abruña, H. D. *Langmuir* **1999**, *15*, 7325.
(19) Sun, S.-G.; Chen, A.-C.; Huang, T.-S.; Li, J.-B.; Tian, Z.-W. *J. Electroanal. Chem.* **1992**, *340*, 213.
(20) Tarnowski, D. J.; Korzeniewski, C. *J. Phys. Chem. B* **1997**, *101*, 253.
(21) Beden, B.; Lamy, C.; de Tacconi, N. R.; Arvia, A. J. *Electrochim. Acta* **1990**, *35*, 691.
(22) Gilman, S. *J. Phys. Chem*. **1964**, *68*, 70.
(23) Bergelin, M.; Herrero, E.; Feliu, J. M.; Wasberg, M. *J. Electroanal. Chem*. **1999**, *467*, 74.
(24) Lebedeva, N. P.; Koper, M. T. M.; Feliu, J. M.; van Santen, R. A. *J. Electroanal. Chem*. **2002**, *524*−*525*, 242.
(25) Lebedeva, N. P.; Koper, M. T. M.; Feliu, J. M.; van Santen, R. A. *J. Phys. Chem. B*, in press.
(26) (a) Xu, J.; Henriksen, P.; Yates, J. T., Jr. *J. Chem. Phys*. **1992**, *97*, 5250. (b) Xu, J.; Yates, J. T., Jr. *J. Chem. Phys*. **1993**, *99*, 725.
(27) Willis, R. F.; Lucas, A. A.; Mahan, G. D. Vibrational properties of adsorbed molecules. In *The Chemical Physics of Solid Surfaces and Heterogeneous Catalysis*; King, D. A., Woodruff, D. P., Eds.; Elsevier: Amsterdam, 1983.
(28) Hoffmann, F. M. *Surf. Sci. Rep*. **1983**, *3*, 107.
(29) Iwasita, T.; Nart, F. C. *Prog. Surf. Sci.* **1997**, *55*, 271.
(30) Hollins, P. *Surf. Sci. Rep.* **1992**, *16*, 51.
(31) Clavilier, J.; Armand, D.; Sun, S. G.; Petit, M. *J. Electroanal. Chem.* **1986,** *205*, 267.
(32) Iwasita, T.; Nart, F. C.; Vielstich, W. *Ber. Bunsen-Ges. Phys. Chem.* **1990**, *94*, 1030.
(33) Gómez, R.; Feliu, J. M.; Aldaz, A.; Weaver, M. J. *Surf. Sci*. **1998**, *410*, 48.
(34) Gómez, R.; Climent, V.; Feliu, J. M.; Weaver, M. J. *J. Phys. Chem. B* **2000**, *104*, 597.
(35) This figure was produced using the BALSAC program, copyright K. Hermann 1991−9, http://w3.rz-berlin.mpg.de/~hermann/hermann/balpam.html.
(36) Herrero, E.; Orts, J. M.; Aldaz, A.; Feliu, J. M. *Surf. Sci.* **1999**, *440*, 259.
(37) (a) Smoluchowski, R. *Phys. Rev*. **1941**, *60*, 661. (b) Wandelt, K. *Appl. Surf. Sci*. **1997**, *111*, 1.
(38) Clavilier, J.; El Achi, K.; Rodes, A. *Chem. Phys*. **1990**, *141*, 1.
(39) Clavilier, J.; El Achi, K.; Rodes, A. *J. Electroanal. Chem.* **1989**, *272*, 253.
(40) Rodes, A.; El Achi, K.; Zamakhchari, M. A.; Clavilier, J. *J. Electroanal. Chem.* **1990**, *284*, 245.
(41) Stonehart, P. *Electrochim. Acta* **1973**, *18*, 63.
(42) Feliu, J. M.; Orts, J. M.; Fernandez-Vega, A.; Aldaz, A.; Clavilier, J. *J. Electroanal. Chem.* **1990**, *296*, 191.
(43) Rodes, A.; Gómez, R.; Feliu, J. M.; Weaver, M. J. *Langmuir* **2000**, *16*, 811.
(44) Shin, J.; Korzeniewski, C. *J. Phys. Chem*. **1995**, *99*, 3419.
(45) Leung, L.-W.; Wieckowski, A.; Weaver, M. J. *J. Phys. Chem*. **1988**, *92*, 6985.
(46) Chang, S.-C.; Weaver, M. J. *J. Chem. Phys*. **1990**, *92*, 4582.
(47) Villegas, I.; Weaver, M. J. *J. Chem. Phys*. **1994**, *101*, 1648.
(48) Chang, S.-C.; Weaver, M. J. *J. Phys. Chem*. **1990**, *94*, 5095.
(49) Chang, S.-C.; Weaver, M. J. *Surf. Sci*. **1990**, *238*, 142.
(50) (a) Illas, F.; Mele, F.; Curulla, D.; Clotet, A.; Ricart, J. M. *Electrochim. Acta* **1998**, *44*, 1213. (b) Curulla, D.; Clotet, A.; Ricart, J. M.; Illas, F. *Electrochim. Acta* **1999**, *45*, 639. (c) Koper, M. T. M.; van Santen, R. A. *J. Electroanal. Chem.* **1999**, *476*, 64. (d) Koper, M. T. M.; van Santen, R. A.; Wasileski, S. A.; Weaver, M. J. *J. Chem. Phys*. **2000**, *113*, 4392.
(51) Kunimatsu, K. *J. Phys. Chem*. **1984**, *88*, 2195.
(52) Head-Gordon, M.; Tully, J. C. *Chem. Phys*. **1993**, *175*, 37.
(53) Bagus, P. S.; Pacchioni, G. *Surf. Sci*. **1990**, *236*, 233.
(54) (a) Wasileski, S. A.; Koper, M. T. M.; Weaver, M. J. *J. Phys. Chem. B* **2001**, *105*, 3518. (b) Wasileski, S. A.; Koper, M. T. M.; Weaver, M. J. *J. Chem. Phys.* **2001**, *115*, 8193. (c) Wasileski, S. A.; Koper, M. T. M.; Weaver, M. J. *J. Am. Chem. Soc.* **2002**, *124*, 2796.
(55) Yoshioka, K.; Kitamura, F.; Takeda, M.; Takahashi, M.; Ito, M. *Surf. Sci.* **1990**, *227*, 90.
(56) Nart, F. C.; Iwasita, T. *Electrochim. Acta* **1996**, *41*, 631.
(57) Lambert, D. K. *J. Chem. Phys.* **1991**, *94*, 6238.
(58) Park, S.; Wasileski, S. A.; Weaver, M. J. *J. Phys. Chem. B* **2001**, *105*, 9719.
(59) (a) Reutt-Robey, J. E.; Doren, D. J.; Chabal, Y. J.; Christman, S. B. *Phys. Rev. Lett*. **1988**, *61*, 2778. (b) Reutt-Robey, J. E.; Chabal, Y. J.; Doren, D. J.; Christman, S. B. *J. Vac. Sci. Technol. A* **1989**, *7*, 2227. (c) Reutt-Robey, J. E.; Doren, D. J.; Chabal, Y. J.; Christman, S. B. *J. Chem. Phys*. **1990**, *93*, 9113. (d) Ma, J.; Xiao, X.; DiNardo, N. J.; Loy, M. M. T. *Phys. Rev. B* **1998,** *58*, 4877.
(60) Hoshi, N.; Tanizaki, M.; Koga, O.; Hori, Y. *Chem. Phys. Lett*. **2001**, *336*, 13.
(61) Koper, M. T. M.; Lebedeva, N. P.; Hermse, C. G. M. *Faraday Discuss.* **2002**, *121*, 301.